Malaysian Journal of Mathematical Sciences 11(2): 165–179 (2017)

MALAYSIAN JOURNAL OF MATHEMATICAL SCIENCES
Journal homepage: http://einspem.upm.edu.my/journal

Finite Element Simulation of Blood Flow Through an Artery Bifurcation: A Mathematical Model

Rajashekhar, C.[1], Manjunatha, G.*[1], and Fabian, B.[2]

[1]*Department of Mathematics, Manipal Institute of Technology, India*
[2]*Department of Physics, Technische University Berlin, Germany*

E-mail: manjunatha.g@manipal.edu
**Corresponding author*

Received: 29th September 2016
Accepted: 3rd March 2017

ABSTRACT

A mathematical model for the flow of human blood through an artery bifurcation is studied using finite element analysis (FEA). The FEA has been applied for a two-dimensional steady flow of an in-viscous fluid through different geometries. The flow through a two-dimensional model of a carotid artery bifurcation has been simulated. The velocity profiles through the bifurcation branches were computed. The validity of the computational method was established by comparing the numerical results with other findings.

Keywords: Pulsatile, Carotid artery, Bifurcation.

1. Introduction

The study of blood flow through bifurcations in the arterial system has been of special interest with certain form of arterial diseases. Bifurcations are often the center of diseases of the blood vessels like atherosclerosis or ruptures of the walls (Guyton (1981)). They can lead to symptoms such as high blood pressure or thrombolyses, which can cause strokes or heart attacks (Arjmandi-Tash et al. (2011)). Atherosclerosis are linked with regions of low flow velocity and it is heavily influenced by the geometry of the bifurcation and the viscosity (Kaluzynski and Liepsch (1995)).

Though simplified two-dimensional geometric idealization yields basic information, an approximate analysis requires the consideration of three-dimensional geometry; because two-dimensional models are unable to show important effects such as secondary motion. The study reveals a complex flow field in which secondary flow plays an important role (Bharadvaj et al. (1982)). Further, Perktold et al. (1991a) discussed the wall shear stress and non-Newtonian flow velocity during the pulse cycle and also numerically analyzed the wall shear stresses and the flow phenomenon in the human carotid artery bifurcation.

Numerical methods are very useful in supporting experimental methods and often enable the determination of flow variable which is difficult to obtain through experiments, e.g. wall shear stresses. A considerable number of numerical studies are carried out for Newtonian and non-Newtonian fluids to analyze the flow in two and three dimensional carotid artery bifurcation (Boileau et al. (2015), Botner et al. (2000), Chakravarty et al. (2000), Chen and Lu (2006), Fany et al. (2009), Jou and Berger (1998), Karner et al. (1999), Lou and Yang (1993), Perktold and Rappitsch (1995), Perktold et al. (1991b), Taewon (2013)). Although these numerical methods provide satisfactory approximations, finite element method was used by many researchers to give better solution for carotid artery bifurcation in Auricchio et al. (2012), Kwack and Masud (2014), Taylor et al. (1998)

A comparative study has been done in Manjunatha et al. (2015) compared the analytical results from the model with that of the experimental values for velocity and flow rates. Zhang et al. (2016) examined the left coronary artery as an exemplification using wall shear stress and wall pressure gradient. Further, Gharahi et al. (2016) enhanced the estimation of hemodynamics of carotid artery by developing computational fluid dynamics analysis using magnetic resonance imaging (MRI). Recently, Urevc et al. (2017) developed a blood viscosity model to predict the blood in the steady-state as a function of viscosity.

The purpose of FEM is to find an expression which becomes minimal when the accurate approximation is inserted. An example for such an expression would be the total energy of the system. For continuum mechanics and especially fluid dynamics, the standard approach is the weighted residual method and since it is hard to find the functional in nonstructural systems. Using variational or weighted residual methods reduces the problem to solving a system of linear equations. When using polynomials as interpolation functions, the system has to be solved for the coefficients. The size of the system of linear equations increases with the order of the polynomial. In general, the approximation becomes accurate for higher order polynomials at the cost of higher computations. Another important aspect when solving the system of linear equation is the inclusion of the boundary conditions. If not imposed before explaining the system, the matrix will be singular.

The goal of this paper is to understand the basics of numerical analysis of the blood flow by finite element analysis. As part of this study, a simple software for FEM was also developed to model the steady flow of viscous incompressible fluids through artery bifurcations. The computed results obtained from a finite element method (velocity and flux) gives the proper agreement with Perktold and Rappitsch (1995), Taylor et al. (1998).

2. Model for Y-bifurcation

The study investigates the flow through a Y-bifurcation of a carotid artery in the neck. In the present two-dimensional model, the carotid artery (CCA) branches into two smaller vessels, the internal carotid artery (ICA) and the external carotid artery (ECA). The bifurcation is symmetric with an angle of 37^0 at the apex between both vessels. The flow ratio is divided at a ratio of 70 : 30 between ICA and ECA respectively. The ICA provides the blood flow to the brain. In the model, the radius of the CCA is taken as 3.3 mm (Perktold and Rappitsch (1995)). The walls at the bifurcation are assumed to bend in a quadratic function towards the ICA and ECA. The ICA is tapered, starting from the radius of the CCA down to a radius of 2.4 mm (Perktold and Rappitsch (1995)) after a distance of 10 mm. The ECA is assumed to be symmetrical. The model for the bifurcation and the resulting mesh is shown in Figure 1.

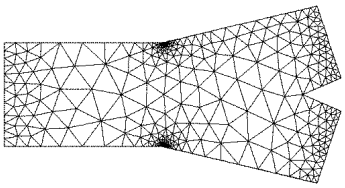

Figure 1: The mesh used for the Y-bifurcation.

3. Formulation

The carotid artery is distensible, and we assume the tapering of the arterial wall radius as the axial distance increases from the apex. Let R and R_I represents the radius of CCA and ICA respectively. The ICA is tapered from 3.3 mm at the neck termed 0.0 mm (axial) into the ICA to 2.4 mm at a point 10.0 mm into the ICA. Analyzing the tapering, the radius of CCA is given by,

$$R = R_0 - Ztan\theta, \tag{1}$$

where R_0 is the undisturbed radius, Z is the location in question, and θ is the angle of tapering. Equation (1) is valid for rigid tube. However, the tube is distensible (elastic like the carotid artery), and radius of ICA is given by,

$$R_I = R\left[1 \pm \in sin\frac{2\pi}{\lambda}(Z - ct)\right], \tag{2}$$

where $\in$ is the amplitude ratio of the distensible wall, λ is the wavelength, c is the wave speed and t is the time.

The flow is pulsatile in the tube, and the arterial motion is sinusoidal. Also, the pressure differences help in the flow of blood and further, into the artery. The wavelength (λ) is not the same in ICA and CCA because the flow velocities in both the tubes are not equal. The Navier-Stokes equations describing the motion of the fluid in the model are taken in radial and axial directions.

$$\rho\frac{\partial\overline{u}}{\partial\overline{t}} = -\frac{\partial\overline{p}}{\partial\overline{r}} + \mu\left[\frac{\partial^2\overline{u}}{\partial\overline{r^2}} + \frac{1}{\overline{r}}\frac{\partial\overline{u}}{\partial\overline{r}} - \frac{\overline{u}}{\overline{r^2}} + \frac{\partial^2\overline{u}}{\partial\overline{z^2}}\right], \tag{3}$$

$$\rho\frac{\partial\overline{v}}{\partial\overline{t}} = -\frac{\partial\overline{p}}{\partial\overline{z}} + \mu\left[\frac{\partial^2\overline{v}}{\partial\overline{r^2}} + \frac{1}{\overline{r}}\frac{\partial\overline{v}}{\partial\overline{r}} + \frac{\partial^2\overline{v}}{\partial\overline{z^2}}\right]. \tag{4}$$

With the continuity equation,

$$\frac{1}{\overline{r}}\frac{\partial}{\partial \overline{r}}\left(r\overline{u}\right)+\frac{\partial \overline{v}}{\partial \overline{z}}=0 \tag{5}$$

Taking dimensionless quantities

$$v=\frac{\overline{v}}{v_0},\ u=\frac{\overline{u}}{u_0},\ p=\frac{\overline{p}}{\rho v_0^2},\ t=\frac{\overline{t}v_o}{R_0},\ z=\frac{\overline{z}}{z_0},\ r=\frac{\overline{r}}{R_0},\ with\ z_0\approx R_0. \tag{6}$$

The Equations (3) and (4) become,

$$\frac{\partial u}{\partial t} = -\frac{\partial p}{\partial r}+\frac{1}{R_e}\left[\frac{\partial^2 u}{\partial r^2}+\frac{1}{r}\frac{\partial u}{\partial r}-\frac{u}{r^2}+\frac{\partial^2 u}{\partial z^2}\right], \tag{7}$$

$$\frac{\partial v}{\partial t} = -\frac{\partial p}{\partial t}+\frac{1}{R_e}\left[\frac{\partial^2 v}{\partial r^2}+\frac{1}{r}\frac{\partial v}{\partial r}+\frac{\partial^2 v}{\partial z^2}\right] \tag{8}$$

4. Discretization

For solving the governing equation, by applying FEM the discretization can be done manually by defining some nodes over the geometry and connecting them to finite elements. A requirement for the finite elements is that each of them should have the same number of nodes. The number of nodes also dictates the choice of the interpolation function. For a two-dimensional linear interpolation function (9), we have three unknown coefficients.

$$\phi_i(x,y)=a_i+b_ix+c_iy \tag{9}$$

To solve the resulting system of linear equations, the number of unknowns has to be equal to the number of nodes. For the linear interpolation function in (9), we would, therefore, need a triangular shape defined by three nodes (Figure 2), because, for the convergence of the solution in FEM the assumed displacement field should be isotropic. This is achieved by using Pascal's triangle. If the components of the displacement field are complete polynomials, it helps to include an appropriate number of terms in the displacement model.

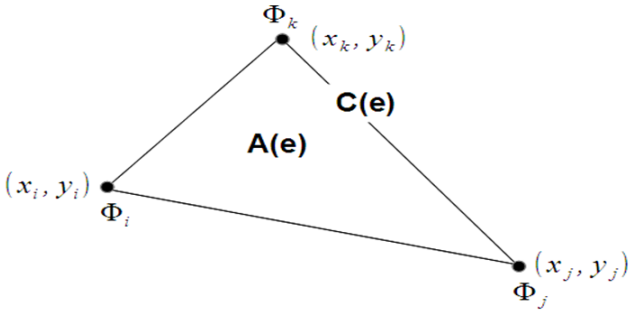

Figure 2: A two-dimensional finite element defined by the three nodes ϕ_i, ϕ_j and ϕ_k.

5. Analysis

By choosing the stream function $\Psi = 1.5\left(-\frac{x^3}{3} + x\right)$. For this, the flow of an in-viscous fluid around a cylinder between two plates is considered, because, we are assuming that the viscosity of blood ($\mu = 0.03$ *Poise*) is constant for a normal healthy person (Guyton (1981)). For further studies, we can apply FEM analysis for varying viscosities. The geometry used is shown in Figure 3.

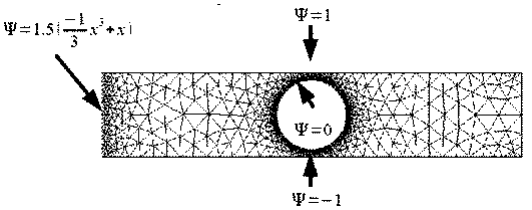

Figure 3: Mesh and boundary conditions used for simulation.

We consider a channel of 10 *cm* by 2 *cm* with a cylinder in the center of radius of 0.83 *cm*. The following boundary conditions are assumed:

Along the upper edge, the stream function is set to a constant value of 1. Along the lower edge, the value is set to -1. Along the boundary of the circle, the stream function is set to zero. For the inflow along the left edge, we assume a parabolic flow profile. Since the velocity is given by the basic equation, the boundary condition for the stream function is the integral of the parabolic flow

profile and it is given by,

$$\Phi(y) = 1.5\left(-\frac{1}{3}x^3 + x\right) \tag{10}$$

The calculated stream function is shown in Figure 4. We can clearly see, how the streamlines bend around the cylinder (Figure 5). The initial parabolic flow profile also develops into a constant flow profile (Figure 6). To visualize this, we derive the flow profile from the stream function. Since the velocity is given by the derivative in the y direction, we can use the differential quotient for the discrete finite elements:

$$u_i = \frac{\Psi_i - \Psi_j}{|x_i - x_j|} \tag{11}$$

The flow profiles for different positions about the left edge are shown in Figure 7. We can clearly observe that the flow changes from a parabolic to a constant profile further away from the left edge. At a distance of 1.2 cm from the left edge, the flow is already linear. (Note that the axial velocity variation is not, in general, parabolic, and in fact reverses in direction close to the wall even tough the total volume flow always remains positive) (Taylor et al. (1998)).

We also derive the flow profile around the cylinder. The velocity profile are shown in Figure 8. As the fluid approaches the cylinder, the velocity decreases in the center while it increases at the sides. As soon as the fluid hits the surface of the cylinder, the speed decreases from the upper wall and increases again towards the cylinder boundary. The effect increases as the distance between the walls and the cylinder decreases. At the minimal distance at $x = 0$ cm, the velocity increases from the wall towards the cylinder. At the same time, an increase in the overall velocity with decreasing distance between wall and the cylinder can be observed (Chattot and Hafez (2015)).

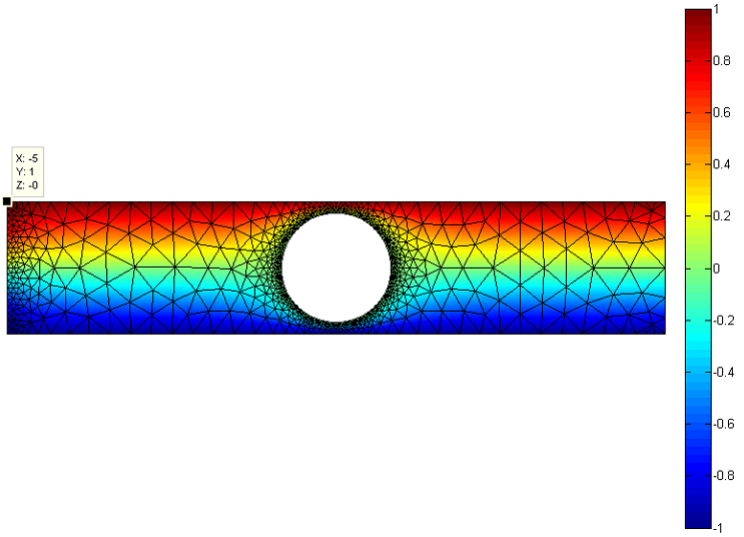

Figure 4: Streamlines of the in-viscous fluid around the cylinder.

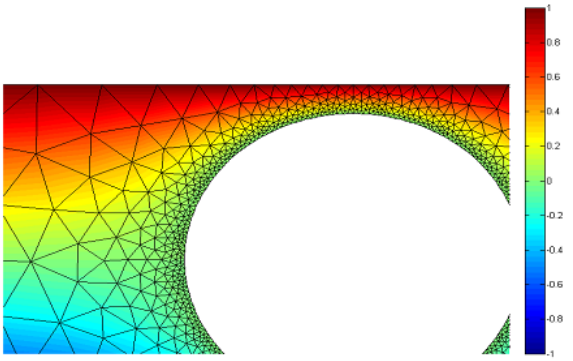

Figure 5: Close up of the streamlines around the cylinder.

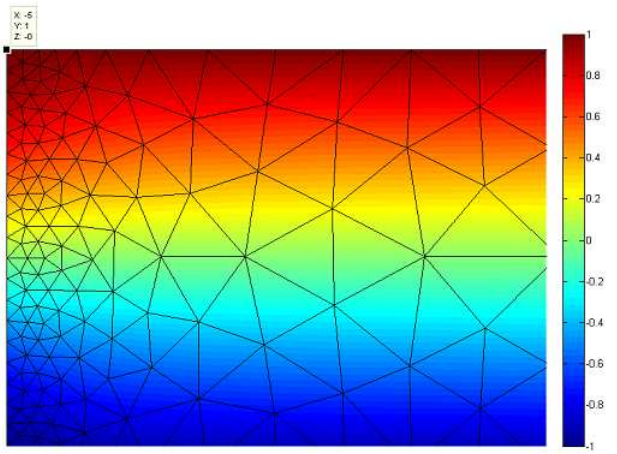

Figure 6: Close up of the streamlines at the transition from parabolic to constant velocity profile.

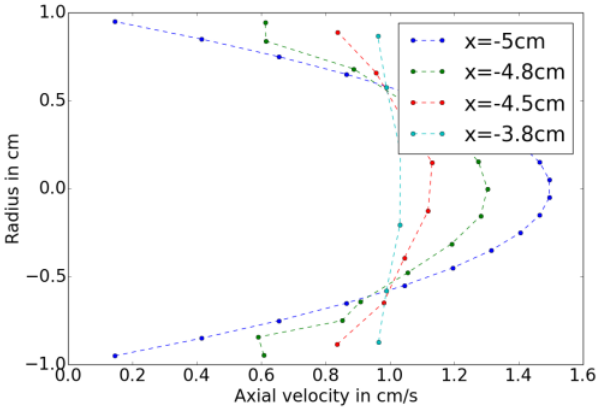

Figure 7: Velocity profiles along the channel at the transition from parabolic to constant profile.

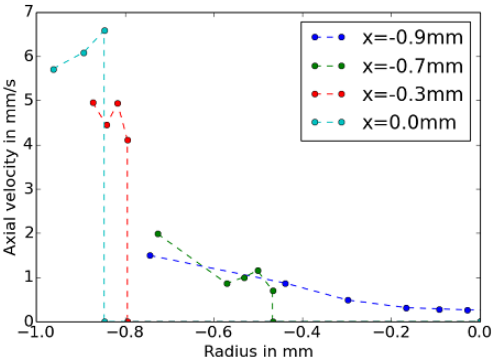

Figure 8: Velocity profiles at different positions along the cylinder.

Another quantity for analysis is the flux. It is defined as the integral of the velocity over the surface of a cross-section.

$$Q = \int_{A(e)} v(x, y, z) dA. \tag{12}$$

In two-dimensional case with radial symmetry, the integral can be simplified as:

$$Q = \pi R \int_{-R}^{R} v(r) dr. \tag{13}$$

Here, R is the Radius of the tube. For the case of finite elements, the velocity distribution becomes discretized and the integral transforms to a sum:

$$Q = \pi R \sum_{i=1}^{N} v_i \Delta r, \tag{14}$$

where N is the number of discrete elements and Δr is the width of an element. The flux for the cylinder is analyzed for different positions along the tube. At the inflow, the value is $s = 6.1544\ cm^3$ and $s = 6.2763\ cm^3$ at the out flow. It can be seen that the flux at the inlet and outlet are the same, thus the total flow is conserved. The small differences in the flux can be explained by errors due to the finite size of the meshing.

5.1 In-viscous flow through a Y-bifurcation

We now consider the in-viscous flow through a Y-bifurcation. For the simulation, the following boundary conditions were used (Figure 9): On the upper walls, the stream function is set to 1, on the lower walls to -1. At the apex, the value is set to 0. For the inflow, we again assume a parabolic flow profile. The resulting streamlines are shown in Figure 10 and 11.

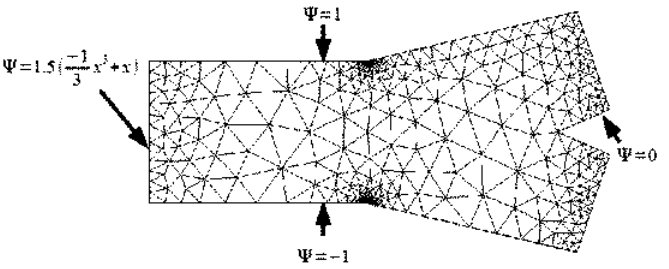

Figure 9: Mesh and boundary conditions used for the simulation.

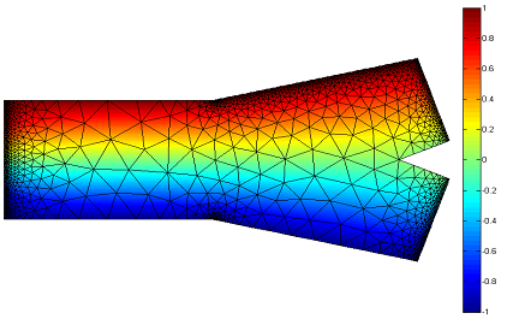

Figure 10: Streamlines along the bifurcation.

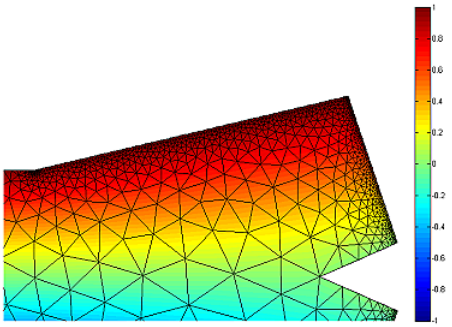

Figure 11: Close-up of the streamlines separating at the apex.

We can see the flow separating at the apex into the ICA and ECA. Through the choice of the boundary conditions, the flow divides symmetrically into both vessels, and this can also be observed in the velocity profiles. Both are symmetrical over the radius of the cross-section of the bifurcation. The velocity profile at the outlet is shown in Figure 12. It clearly shows the fluid having a higher velocity towards the apex. We find that the flux at the inlet is equally divided between ICA and ECA. The value at the inlet is 6.27 cm^3, and that in the ICA and ECA is around 3.14 cm^3. This is expected since the flow profiles have been already symmetric.

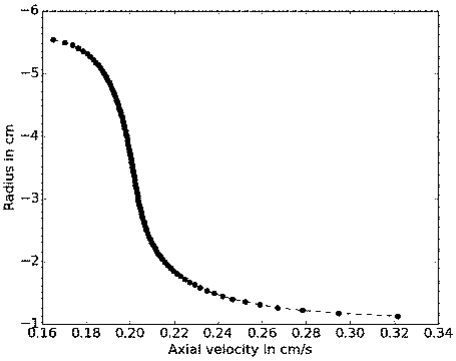

Figure 12: Velocity profile at the outlet of the ECA.

6. Conclusion

The mathematical model for the flow of blood in carotid artery bifurcation have been studied by using finite element simulation. The present model shows the functionality of the developed finite element program. The flow profiles for a in-viscous fluid (constant viscosity) were computed for different geometries. The standard test of flow past a cylinder showed the expected flow profiles. Furthermore, the computed velocity profiles and flux will give a good agreement with the existing models (Perktold and Rappitsch (1995), Taylor et al. (1998)).

References

Arjmandi-Tash, O., Razavii, S. E., and Zanbouri, R. (2011). Possibility of atherosclerosis in an arterial bifurcation model. *Bioimpacts*, 1:225–228.

Auricchio, F., Conti, M., Ferrara, A., Morganti, S., and Reali, A. (2012). Patient-specific finite element analysis of carotid artery stenting: a focus on vessel modeling. *International Journal for Numerical Methods in Biomedical Engineering*, 29:645–664.

Bharadvaj, B. K., Mabon, R. F., and Giddens, D. P. (1982). Steady flow in a model of the human carotid bifurcation, part i - flow visualization. *Journal of Biomechanics*, 15:349–362.

Boileau, E., Nithiarasu, P., Blanco, P. J., Muller, L. O., Fossan, F. E., Hellevik, L. R., Donders, W. P., Huberts, W., Willemet, M., and Alastruey, J. (2015). A benchmark study of numerical schemes for one-dimensional arterial blood flow modelling. *International Journal for Numerical Methods in Biomedical Engineering*, 31:1–33.

Botner, R., Rappitsch, G., Scheidegg, M. V., Liepsch, D., Perktold, K., and Veisegr, P. (2000). Hemodynamics in the carotid artery bifurcation, a comparison between numerical solution and in vitro mri measurements. *Journal of Biomechanics*, 33:137–144.

Chakravarty, S., Mandal, P. K., and Mandal, A. (2000). Mathematical model of pulsatile blood flow in a distensible aortic bifurcation subject to body acceleration. *Int. J. Engg. Science*, 38:215–238.

Chattot, J. J. and Hafez, M. M. (2015). *Theoretical and Applied Aerodynamics*. Springer, Netharland, 1st edition.

Chen, J. and Lu, X.-Y. (2006). Numerical investigation of the non-newtonian pulsatile blood flow in a bifurcation model with a non planar branch. *Journal of Biomechanics*, 35:818–832.

Fany, Y., Jiand, W., Zou, Y., Li, J., Chen, J., and Deng, X. (2009). Numerical simulation of pulsatile non-newtonian flow in the carotid artery bifurcation. *Acta Mechanica Sinica / Lixue Xuebao*, 25:249–255.

Gharahi, H., Zambrano, B. A., Zhu, D. C., DeMarco, J. K., and Baek, S. (2016). Computational fluid dynamic simulation of human carotid artery bifurcation based on anatomy and volumetric blood flow rate measured with magnetic resonance imaging. *International Journal of Advances in Engineering Sciences and Applied Mathematics*, 8:40–60.

Guyton, A. (1981). *Textbook of Medical Physiology.* Elsevier, Pennsylvania, 11th edition.

Jou, L. D. and Berger, S. A. (1998). Numerical simulation of the flow in the carotid bifurcation. theoretical and computational fluid dynamics. *Theoretical and Computational Fluid Dynamics*, 10:239–248.

Kaluzynski, K. and Liepsch, D. (1995). The effect of wall roughness on velocity distribution in a model of the carotid sinus bifurcation analysis of laser and ultrasound doppler velocity data. *Technology and Health Care*, 3:153–159.

Karner, G., Perktold, K., Hoter, M., and Liepsch, D. (1999). Flow characteristics in an anatomically realistic complaint carotid artery bifurcation model. *Computer methods in Biomechanics and Biomedical Engineering*, 2:171–185.

Kwack, J. and Masud, A. (2014). A stabilized mixed finite element method for shear-rate dependent non-newtonian fluids: 3d benchmark problems and application to blood flow in bifurcating arteries. *Computational Mechanics*, 53:751–776.

Lou, Z. and Yang, W. J. (1993). A computer simulation of blood flows at the aortic bifurcation with flexible walls. *J. Biomech. Engg.*, 115:306–315.

Manjunatha, G., Basavarajappa, K. S., and Katiyar, V. K. (2015). Mathematical modelling on pulsatile flow in carotid artery bifurcation in reference to atherosclerosis with varying frequencies. *Global Journal of Pure and Applied Mathematics*, 11:3467–3475.

Perktold, K. and Rappitsch, G. (1995). Computer simulation of local blood flow and vessel mechanics in a compliant carotid artery bifurcation model. *Journal of Biomechanics*, 28:845–856.

Perktold, K., Resch, M., and Florian, H. (1991a). Pulsatile non-newtonian flow charecteristics in a three dimensional human carotid bifurcation model. *Journal of Biomechanical Engineering*, 113:464–475.

Perktold, K., Resch, M., and Peter, R. . (1991b). Three dimensional numerical analysis of pulsatile flow and wall shear stress in the carotid artery bifurcation. *Journal of Biomechanics*, 24:409–420.

Taewon, S. (2013). Numerical simulations of blood flow in arterial bifurcation models. *Korea - Australia Rheology Journal*, 25:153–161.

Taylor, C. A., Hughes, T. J., and Zarinsb, C. K. (1998). Finite element modeling of blood flow in arteries. *Computer Methods in Applied Mechanics and Engineering*, 158:155–196.

Urevc, J., Zun, I., Brumen, M., and Stok, B. (2017). Modeling the effect of red blood cells deformability on blood flow conditions in human carotid artery bifurcation. *Journal of Biomechanical Engineering*, 139:011011–11.

Zhang, B., Jin, Y., Wang, X., Zeng, T., and Wang, L. (2016). Numerical simulation of transient blood flow through the left coronary artery with varying degrees of bifurcation angles. *Journal of Mechanics in Medicine and Biology*, 17:1750005–11.